Cooperative Structural Dynamics and a Novel Fidelity Mechanism in Histidyl-tRNA Synthetases‡

Xiayang Qiu,*,§ Cheryl A. Janson,|| Michael N. Blackburn,§ Inderjit K. Chhohan,|| Martin Hibbs,|| and Sherin S. Abdel-Meguid§

Department of Structural Biology and Department of Protein Biochemistry, SmithKline Beecham Pharmaceuticals, King of Prussia, Pennsylvania 19406

Received March 2, 1999; Revised Manuscript Received June 7, 1999

ABSTRACT: The crystal structure of the *Staphylococcus aureus* histidyl-tRNA synthetase apoprotein has been determined at 2.7 Å resolution. Several important loops in the active site either become disordered or adopt very different conformations compared to their ligand-bound states. These include the histidine A motif (Arg257−Tyr262) that is essential for substrate recognition, a loop (Gly52−Lys62) that seems to control the communication between the histidine and ATP binding sites, the motif 2 loop (Glu114−Arg120) that binds ATP, and the insertion domain that is likely to bind tRNA. These ligand-induced structural changes are supported by fluorescence experiments, which also suggest highly cooperative dynamics. A dynamic and cooperative active site is most likely necessary for the proper functioning of the histidyl-tRNA synthetase, and suggests a novel mechanism for improving charging fidelity.

Aminoacyl-tRNAs[1] (charged tRNAs) are required during the translation step of protein synthesis. They recognize mRNA codons with their anticodons, and allow the charged amino acids to be added accurately to the growing peptide chain. Each amino acid is charged onto its cognate tRNA by a specific aminoacyl-tRNA synthetase. The reaction is usually carried out in two steps; the amino acid is first condensed with ATP to form aminoacyl-adenylate, and then transferred to tRNA to form the final product (*1*). Aside from catalytic efficiency, fidelity is another key element of the charging reaction. The active sites of aminoacyl-tRNA synthetases not only have to bind amino acids with sufficient affinity but also require high specificity to minimize the activation and charging of incorrect amino acids. Mischarged tRNAs would introduce incorrect amino acids into nascent protein products, resulting in disruption of the normal folding and activity of these proteins (*2*).

Twenty aminoacyl-tRNA synthetases exist in most organisms. They are evenly divided into two classes by signature motifs in their catalytic domains (*3*). The catalytic domains of class I synthetases exhibit a Rossmann fold and are characterized by the presence of HIGH and KMSKS motifs that are essential for ATP interaction. Class II synthetases have catalytic domains comprised of a six-stranded antiparallel β-sheet and are identified through three conserved motifs. Motif 1 is implicated in dimer formation, while motifs 2 and 3, each containing an arginine, are known to interact with ATP (see ref *3* for motif definitions). Histidyl-tRNA synthetase (HisRS), catalyzing the charging of histidine onto its cognate $tRNA^{His}$, is a homodimer of about 95 kDa. It is a class II aminoacyl-tRNA synthetase as all three motifs are present. It has been further grouped into subclass IIa, along with seryl-, prolyl-, threonyl-, and some glycyl-tRNA synthetases on the basis of sequence similarities in the C-terminal anticodon-binding domain (*4*). HisRS has two additional motifs, histidine A (HisA, RGLDYY) and histidine B (HisB, GGRYDG), both of which are conserved among all known HisRS (*5*−*7*). Crystal structures of *Escherichia coli* HisRS in complex with histidyl-adenylate (*5*) or with histidinol and ATP (*6*) have been reported; so have the *Thermus thermophilus* structures in complexes with histidine or with histidyl-adenylate (*7*). They all contain the class II and subclass IIa signature modules: the antiparallel β-sheet catalytic domain and the C-terminal α/β anticodon-binding domain. A 60-residue insertion domain, in position to bind the tRNA acceptor stem, is visible in the *T. thermophilus* structures but is disordered in the *E. coli* structures. The HisA and HisB motifs interact intimately with the substrate histidine. The essential arginine in the HisA motif was observed to bind the α-phosphate and lies near the histidine carboxylate. The arginine is a likely catalytic residue, replacing the essential divalent metal ion (Mg^{2+}) in other class II tRNA synthetases.

Here we report the crystal structure of the apo *Staphylococcus aureus* histidyl-tRNA synthetase. Unlike the *E. coli* and *T. thermophilus* HisRS structures, our structure is determined in the absence of ligand. Comparisons of the apo and ligand-bound structures reveal considerable conformational changes in the active site. These changes are ligand-induced and presumed to occur in a highly cooperative

‡ The PDB file name is 1EQ0.

* To whom correspondence should be addressed. Telephone: (610) 270-4589. Fax: (610) 270-4091. E-mail: xiayang_qiu-1@sbphrd.com.

§ Department of Structural Biology.

|| Department of Protein Biochemistry.

[1] Abbreviations: HisRS, histidyl-tRNA synthetase; HisA, histidine A motif; HisB, histidine B motif; SI motif, small interface motif; IleRS, isoleucyl-tRNA synthetase; TyrRS, tyrosyl-tRNA synthetase; tRNA, transfer RNA; SerRS, seryl-tRNA synthetase; GlyRS, glycyl-tRNA synthetase; AspRS, aspartyl-tRNA synthetase; GlnRS, glutaminyl-tRNA synthetase; rms, root-mean-square.

10.1021/bi990482v CCC: $18.00
Published on Web 08/28/1999

Table 1: Data Acquisition and Refinement Statistics

maximum resolution (Å)	2.7
no. of observations	136360
no. of unique reflections	28925
redundancy	5
completeness (%)	100
R_{merge}	0.193
refinement resolution (Å)	7.0−2.7
no. of reflections in refinement	19332
no. of protein atoms	5903
no. of solvent atoms	100
R-factor	0.192
R_{free}	0.270
estimated coordinate error by SIGMAA (Å) (*8*)	0.3
rms deviations	
bonds (Å)	0.013
angles (deg)	2.0
dihedrals (deg)	23.6
impropers (deg)	1.6
no. of observed residues	637
disordered residues	
molecule 1	52−62, 114−120, and 207−218
molecule 2	52−62, 114−120, 172−230, and 420

fashion. The magnitude of that in HisRS is greater than any previously reported for tRNA synthetases.

EXPERIMENTAL PROCEDURES

Protein Expression, Purification, and Crystallization. *S. aureus* HisRS was cloned from a genomic library using a synthetic oligo-DNA with a known sequence (gi:2580431). It was subcloned into the pDB575 vector for overexpression in *E. coli* DH5α cells. The induction was carried out at 37 °C with 1 mM IPTG. The cytosolic fraction of *E. coli* cells, containing 8.5% HisRS, was centrifuged and the supernatant applied to a Source 15Q column. Proteins were eluted using a 0.1 to 0.5 M linear NaCl gradient, with HisRS eluted at 0.18 M NaCl and at 85% purity. A subsequent phenyl-Sepharose step, eluted with a 1.7 to 0.0 M $(NH_4)_2SO_4$ gradient, improved the purity to 95%. The sample was concentrated to 8 mg/mL in 20 mM Tris (pH 7.5), 0.2 M NaCl, 1 mM EDTA, and 1 mM DTT using an Amicon YM10 membrane and stored at −70 °C. More details will be described elsewhere (M. Hibbs et al., in preparation). Crystals were grown at room temperature using the sitting-drop method. The well solution contained 0.1 M sodium citrate buffer (pH 5.6), 0.2 M sodium/potassium tartrate, and 1.8 M $(NH_4)_2SO_4$. The drop solution was a 1:1 mixture of the protein and the well solutions. Crystals appeared in several days, all having an unusual spherical shape (∼0.3 mm in diameter).

Data Collection and Analysis. Since the crystals diffracted weakly, a synchrotron source was essential for obtaining usable data. A 2.7 Å data set was collected at the Advanced Photon Source beamline 17-ID (IMCA-CAT) from a single frozen crystal. The cryoprotectant contained 80% crystallization well solution and 20% glycerol. The mosaicity of the crystal was 0.6°. Fine ω oscillations (0.3° per image) were used in data acquisition, and the data were processed with the program SAINT. The data set is nearly 100% complete, with about 5-fold redundancy (Table 1). A large portion of the data appeared to have zero intensity, indicating a pseudosymmetry problem. As a result, the overall R_{merge} was as high as 19%, whereas the R_{merge} of stronger reflections was about 8%. The crystals were found to belong to the hexagonal space group $P6_5$ (or $P6_1$) with the following cell dimensions: $a = b = 125.7$ Å and $c = 116.0$ Å. There is a dimer in the asymmetric unit, and the estimated solvent content is 55%. It was necessary to exclude the zero intensity in the data, which was further complicated by a severe underestimation of $\sigma(I)$ by SAINT. After evaluation of various data statistics, a conservative $\sigma(I)$ cutoff [$5\sigma(I)$] was used. This retained about 70% of the data for further structure solution and refinement. Self-rotation and native Patterson maps were calculated. There was no apparent non-origin peak in either of the maps.

Structure Solution. The amino acid sequence of *S. aureus* HisRS is 40% identical to that of the *E. coli* HisRS. The crystal structure was determined by molecular replacement using the program AMORE (*8*) with the *E. coli* HisRS (*5*) dimer as the search model. The search model included the side chains of conserved amino acids, and alanines where the sequences diverge. Data from 8.0 to 4.0 Å resolution were used in the searches. The rotation solution was the highest peak of 12.4 in height, compared to 7.3 for the second highest peak. Space group $P6_5$ was deduced from translation searches. The correct solution had an *R* factor of 51.4% and a correlation coefficient of 8.7. After rigid-body refinement, the *R* factor was reduced to 50.4% and the correlation coefficient became 12.9. Solvent flattening and 2-fold averaging were then carried out to 3.2 Å resolution with programs in the CCP4 suite (*8*), resulting in an interpretable electron density map.

Model Building and Refinement. The noncrystallographic 2-fold axis of the HisRS dimer was found at (1/2, 0) and parallel to the *Z*-axis. Since the pseudo-2-fold coincided with an exact 2_1 axis, a pseudo-1/2 translation along *Z* was created, resulting in about 50% of the reflections having near-zero intensity. The two monomers were built independently. Further averaging did not improve the electron density maps. Five percent of the data was set aside for R_{free} validation. Iterative cycles of model building and refinement using XPLOR (*9*) led to the final model (Table 1 and Figure 1). Except for divergent loop regions, tight noncrystallographic restraints (100 or 50 kcal mol^{-1} $Å^{-2}$ for main or side chain atoms) were used throughout the refinement. The root-mean-square (rms) difference between the monomers is 0.1 and 0.4 Å for main and side chain atoms, respectively. Only Glu328, in a mobile loop connecting the N- and C-terminal domains, is in a disallowed region of the Ramanchandran plot. Molecule 1 (yellow in Figure 2A) is better ordered in the dimer and is used for most of the discussions.

Fluorescence Spectrum. Fluorescence measurements were performed with an SLM 8000C spectrofluorometer with excitation at 280 or 290 nm when the sample contained ATP or AMP-PNP. Excitation and emission band-passes were set to 1 nm. Uncorrected emission spectra were taken at room temperature, 22 °C, with an integration time of 3−5 s. Multiple spectra were recorded and averaged to improve the quality of the data. Fluorescence intensities from independent experiments could be reproduced to within 2%. The spectrum of the buffer, 20 mM Tris, 0.1 M NaCl, and 10 mM $MgCl_2$ (pH 8.0), was recorded and subtracted from protein sample spectra to correct for the small Raman peak. Titrations were

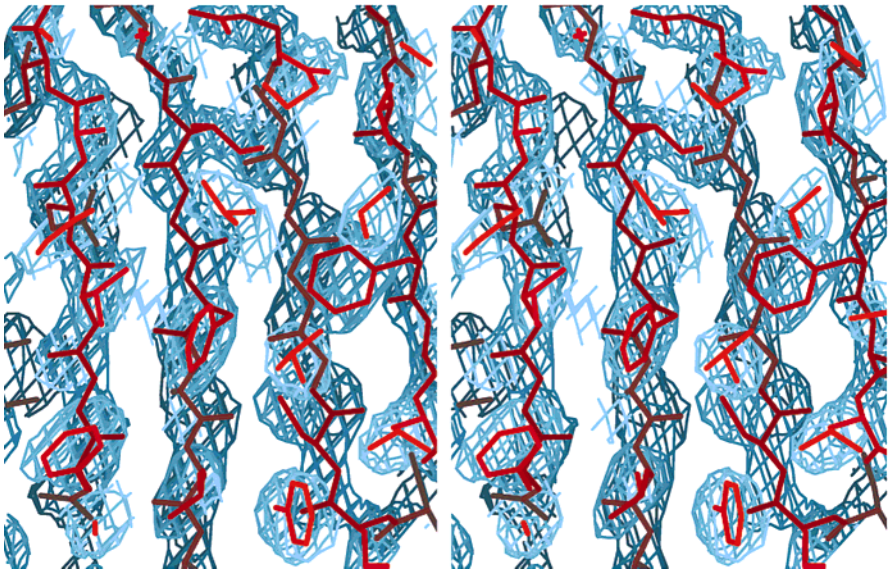

FIGURE 1: Stereoview of the electron density at the class-defining β-sheet region. The $2F_o - F_c$ density was contoured at 1.5σ and plotted with the program XTALVIEW (*10*).

performed by addition of small volumes of the ligand, to a maximum of 10% of the sample volume, and the spectral intensities were corrected for dilution.

RESULTS

Overall Structure. Like many other aminoacyl-tRNA synthetases, HisRS is active as a homodimer. As with the *E. coli* and *T. thermophilus* enzymes (*5*−*7*), the *S. aureus* HisRS monomer contains three domains (Figure 2B). The N-terminal catalytic domain (Met1−Asp168, Leu227−Glu319) has an eight-stranded β-sheet, with the central six strands forming the antiparallel β-sheet that is conserved among all class II synthetases. The front of the β-sheet is mostly open to allow substrate entry, while the back is well protected by helices and flanking loops (Figure 2B). Superposition of the 58 Cα atoms comprising the β-sheet gives an rms difference of 1.2 Å between *S. aureus* HisRS and either *E. coli* or *T. thermophilus* HisRS, and 0.6 Å between the *E. coli* and *T. thermophilus* structures. The C-terminal subclass-defining domain (Leu330−Lys420) has a mixed five-stranded β-sheet and four helices. The helical insertion domain (Met169−Phe226) in our homodimer is ordered in one monomer (Mol 1) but disordered in the other due to crystal packing differences.

The two HisRS molecules in the dimer interact in a side-by-side fashion with their C-terminal domains swapped (Figure 2A). One part of the dimer interface is between the catalytic domain of one monomer and the C-terminal domain of the other monomer. This interface is mostly hydrophilic. The other part of the interface (top middle in Figure 2A) is more hydrophobic and includes structural elements from the N-terminal loop (Met1−Leu12) and a small interface (SI) motif (Phe43−Leu77). The SI motif, shown in magenta in Figure 2B, is present in all class IIa synthetases (*5*). It includes part of motif 1 and an insertion between motifs 1 and 2. The two SI motifs interact intimately in the HisRS dimer, and the interaction is likely important for the HisRS mechanism, as will be discussed.

In the refinement of the *S. aureus* HisRS structure, all domains were allowed to move freely with respect to each other. The relative domain orientations are nearly identical in the two independently determined monomers. However, when the core β-sheets from the three different HisRS are superimposed, orientations of their C-terminal domains differ by 8−15° (Figure 3). At the remote end of these domains, the Cα positions shift as much as 8 Å (*S. aureus* vs *E. coli*), 14 Å (*S. aureus* vs *T. thermophilus*), or 8 Å (*E. coli* vs *T. thermophilus*). An even more significant movement occurs to the highly mobile insertion domain. To reach the same position in the ligand-bound *T. thermophilus* structures, this domain in our apo structure has to rotate more than 30° around its hinge (residues 168 and 227), bringing the domain 12 Å closer to the active site (Figure 3).

While positions of the SI motifs in all the reported structures are nearly identical (Figure 3), a 10° rotation of this motif is observed in our apo HisRS structure. As a result, the β-hairpin's Cα atoms move about 5 Å. Since the SI motif involves both the active site and the dimer interface, the observed conformational change may implicate a communicational path between the two active sites of the dimer.

Conformational Changes in the Histidine Binding Pocket. The most significant ligand-induced conformational changes occur in the histidine binding pocket (Figure 3). In the ligand-bound structures, the binding pocket is a narrow cavity that is more than 20 Å deep. Atoms lining the pocket provide an intricate network of hydrogen bonding interactions as well as van der Waals contacts with the substrate histidine (*5*, *7*). In our apo structure, this pocket becomes wide open and appears to require notable conformational changes to form a complementary binding pocket for histidine. The changes seen in the apo structure are centered at the HisA motif loop (257-RGLDYY-262) (Figure 2B). There are differences in the loop structure itself, but the overall conformational change can be described as a 30° outward hinge rotation, resulting in an average 6 Å shift in Cα positions (Figure 4A). This is the first structural evidence of such a dynamic amino acid recognition pocket in tRNA synthetases. The only relevant example is *T. thermophilus* AspRS, in which a single His442 side chain rotates in response to aspartic acid binding (*12*). However, the aspartic acid pocket itself is not dynamic,

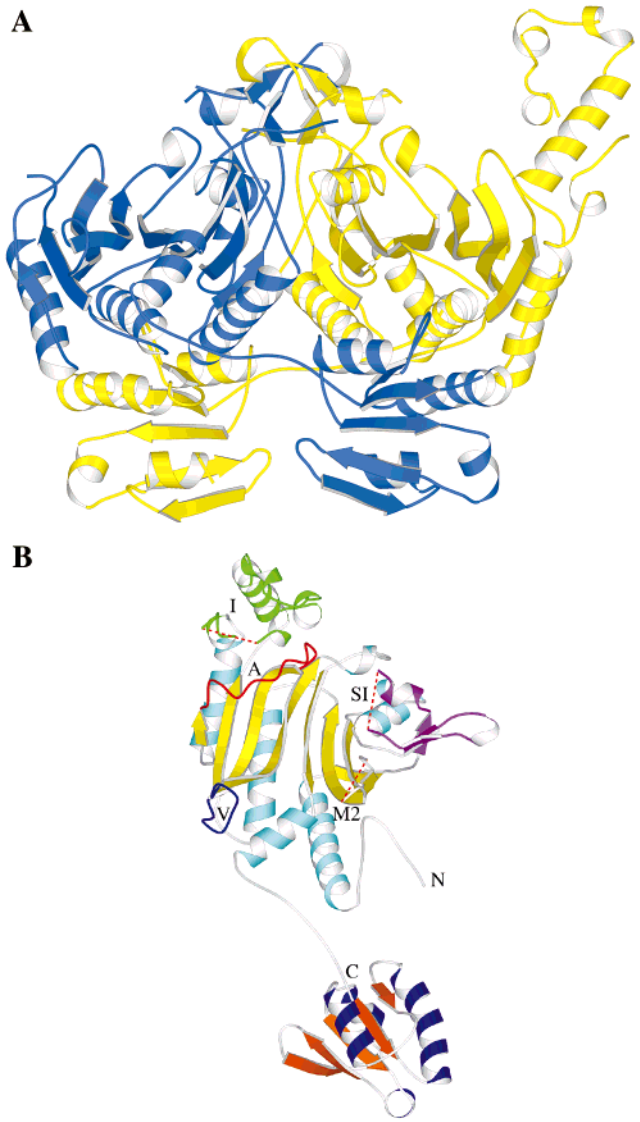

FIGURE 2: Ribbon diagrams of the apo *S. aureus* HisRS structure. (A) The HisRS dimer viewed perpendicular to the 2-fold axis. Molecule 1 is yellow and molecule 2 blue. (B) The HisRS monomer. The catalytic domain is yellow (strands) and cyan (helices). The C-terminal domain is orange (strands) and purple (helices). The insertion domain is green and labeled as I. The small interface motif is magenta and labeled as SI. The HisA motif is red and labeled as A. The loop of residues 273−280 is blue and labeled as V. Dashed red lines connect the missing loops. N- and C-termini are also labeled as N and C, respectively. This figure was drawn with MOLSCRIPT (*11*).

and the recognition role of His442 is probably limited because the same aspartic oxygen is already making a better interaction with Arg483 (*12*). The HisA motif is absolutely conserved among all histidyl-tRNA synthetases and contains at least three essential residues. In the liganded structures, Tyr262 and Tyr261 make hydrogen bonds with the histidine ligand's ND1 atom and amino nitrogen, respectively, and Arg257 contacts both Tyr262 and the ATP α-phosphate. The three residues in the apo structure are shifted 2.3 (Tyr262), 6.6 (Tyr261), and 2.6 Å (Arg257), compared to their counterparts in the *T. thermophilus* HisRS−histidine complex (*7*). In contrast, the HisB motif (286-GGRYDG-291) hardly moves. Differences of about 1.5 Å are visible for the "TXE" (80-EGT-82 in HisRS) loop that binds the amino group of the histidine ligand, as well as the part of motif 2 that provides two ligand-interacting residues, Glu130 (binds NE2 of the ligand) and Gln126 (binds the carboxylate of the ligand).

Other Changes in the Active Site. In all ligand-bound structures (*5*−*7*), the HisA loop also provides numerous contacts to a loop comprising residues Gly52−Lys62. This loop, called the SI loop in this report, is disordered in our structure (Figure 4B). This suggests that the loop is dynamic, and requires support from the HisA loop for stability. Within the loop, the conserved Lys62 (Figure 4C) has been suggested to interact with tRNA (*7*). Any change in the positioning of the loop would affect the orientation of the entire SI motif, and subsequently the dimer interface. From these analyses, it appears that the HisA and SI motifs work cooperatively, and act in concert during catalysis.

In our apo structure, there is another disordered loop (Glu114−Arg120) immediately to the right of the SI loop (Figure 4B). There are close interactions between this loop and the SI loop in HisRS−adenylate complex structures (*5*, *7*), which also suggests cooperativity between them. This is the so-called motif 2 (M2) loop that is in proximity with several essential motif 2 residues. For example, Arg112 is the residue that binds the α- and β-phosphates (*6*), and Phe124 is the one that makes ring-stacking interactions with the adenine moiety of ATP in the liganded structures (*6*, *7*). Within the motif 2 loop, Glu114 forms a hydrogen bond with the exocyclic amino group of adenine, while Arg120 interacts with the γ-phosphate (*6*). The motif 2 loop is also disordered in the absence of the adenosine moiety in the HisRS−histidine complex structure (*7*). Therefore, it is an essential ATP-binding element in HisRS, and probably requires the presence of ATP to assume a stable conformation.

There is yet another loop (Asn273−Ile280) with notable differences in our structure. Unlike other aforementioned loops, sequences of this loop are not conserved, with a three-residue insertion in *S. aureus* HisRS (Figure 4C). Although the loop is in the vicinity of the ATP binding site, it does not interact with the substrate directly. The equivalent loop is disordered in the *E. coli* HisRS−adenylate complex structure, further refuting its role in ATP recognition. It is possible that this loop becomes ordered upon tRNA binding. Most likely, differences in its structure are due only to species differences.

Fluorescence. There is only one tryptophan (Trp19) in *S. aureus* HisRS. The fluorescence spectra of HisRS with excitation at 280 nm indicate that the tryptophan is responsible for most of the signal, with a small shoulder at about 303−305 nm from tyrosine fluorescence (Figure 5A). When only tryptophan is excited at 290 nm, the emission maximum shifts slightly from 331 to 333 nm. Addition of histidine produces a substantial blue shift of 3 nm. The difference in the signal between these spectra has a maximum at 350 nm, which corresponds to the fluorescence of the tryptophan exposed to solvent. This shift indicates that histidine binding perturbs the environment of the tryptophan and that the tryptophan in the unliganded enzyme is moved into a less polar environment in the histidine-liganded enzyme. The perturbation of the tryptophan signal also provides a handle for measuring the binding affinity for binding of histidine to the enzyme, which gives an apparent K_d of 1.2 mM from titration experiments (Figure 5B). The decrease in fluorescence intensity at saturating concentrations of histidine is

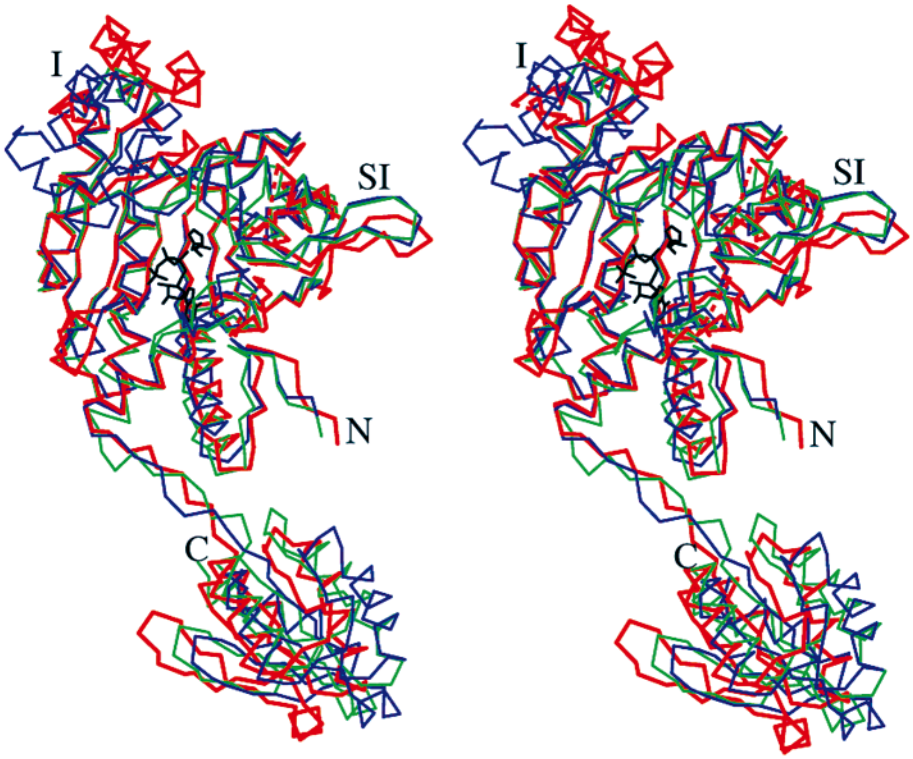

FIGURE 3: Stereoview of Cα superposition of the three HisRS structures. The view is the same as that shown in Figure 2B, and the figure was generated by superimposing the 58 core β-sheet α-carbon atoms of the structures. *S. aureus* HisRS is red, *E. coli* HisRS green, *T. thermophilus* HisRS blue, and histidinol−ATP black. Dashed red lines connect the missing loops in the *S. aureus* apo structure. N and C are the N- and C-termini, respectively. I represents the insertion domain, and SI denotes the small interface motif.

16−17% and is independent of the addition of nucleotide analogues. Addition of 0.2 mM histidine in the presence of added ATP results in a time-dependent shift in tryptophan fluorescence (data not shown), which may indicate the formation of histidyl-adenylate. The fluorescence spectra of the enzyme complexed with histidine, histidine and AMP-PNP, or histidine and ATP were nearly identical, indicating that the binding of histidine and the other ligands leads to the same alteration of the tryptophan environment. ATP or AMP-PNP, however, appears to increase the histidine binding affinity (K_d) to about 0.5 mM (Figure 5B). Since the measurement error is within 2%, this change in binding affinity is significant and suggests some degree of cooperativity between the binding of histidine and ATP.

DISCUSSION

Ligand-Induced Conformational Changes. We believe that the observed structural changes in the HisRS active site are ligand-induced, and not artifacts of species differences, crystallization conditions, or crystal packing. The amino acid sequence homologies are high among the three HisRS with known structures (Figure 4C). Within the catalytic domain, 33% of the *S. aureus* residues are identical to both of the other species, while 56% of the *S. aureus* residues are identical to at least one of the other species. There are only four small gaps in this alignment, with the biggest having a three-residue insertion in the loop of residues 273−280 (V). Moreover, the pairwise sequence identities are nearly the same: 40% between *S. aureus* and *E. coli*, 42% between *S. aureus* and *T. thermophilus*, and 42% between *T. thermophilus* and *E. coli*. Since the liganded *E. coli* and *T. thermophilus* structures are very similar (Figure 3) (*7*), there is no reason to believe that a liganded *S. aureus* structure would be much different from the two, or an apo *E. coli* or *T. thermophilus* structure would be very different from our apo structure. This is especially true for the HisA motif and SI loop because their structures are nearly identical in all liganded structures, are in an open conformation in our apo structure, are not involved in intermolecular interactions and crystal packing, and have sequence identities of 100 and 73%, respectively. Therefore, the observed changes in the active site are ligand-induced and may be applied to all three HisRS species.

Our crystallization conditions, primarily with 2 M $(NH_4)_2SO_4$, are similar to those of *T. thermophilus* HisRS (*7*). The nearly identical structures of the *E. coli* (crystallized from mainly PEG) (*5*) and *T. thermophilus* HisRS suggest insensitivity to crystallization conditions. We have also analyzed all the crystal packing interactions in the lattice. The insertion and C-terminal domains are flexible (*5*−*7*) and involved in contacts with neighboring molecules. However, the flexibility and packing differences do not seem to affect the HisA and SI loops in the liganded HisRS structures. Despite the large differences in the insertion and C-terminal domains, the HisA loops have similar structures in the two independently determined apo HisRS monomers. Thus, crystal packing is probably not a factor in the HisA and SI loop changes. The positioning and the magnitude of structural changes for the insertion domain suggest its correlation to ligand binding. The C-terminal domain does not exhibit a sufficient change for drawing a link to ligand binding, but its flexibility does not contradict the possibility of ligand-induced changes. Ligand-induced conformational changes have been observed in the so-called "flipping loop" of class

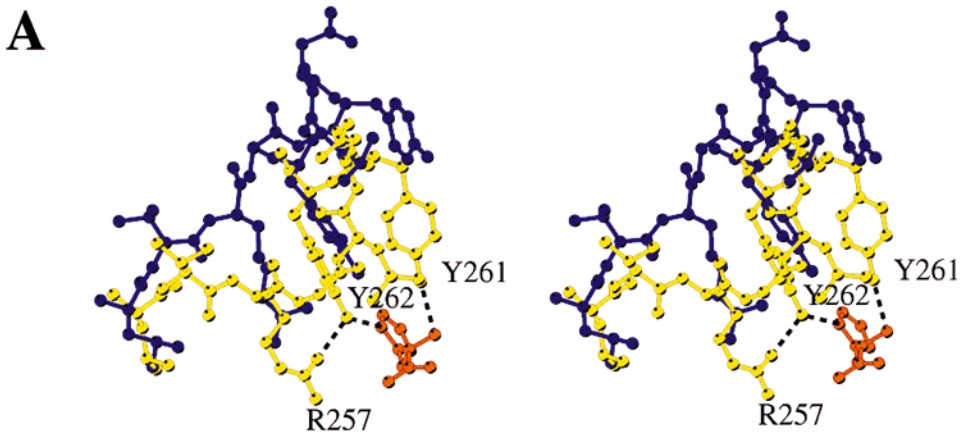

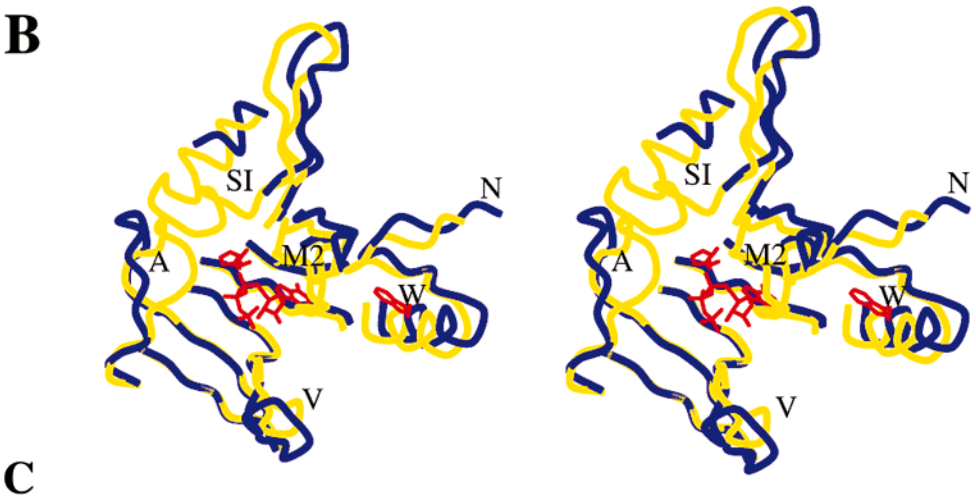

C

```
                                                                SI
Sa    MIKIPRGTQDILPEDSKKWRYIENQLDELMTFYNYKEIRTPIFESTDLFARGVGDSTDVVQKEMYTFKDKGDRSITLRPEGTA  83
Ec AKNIQAIRGMNDYLPGETAIWQRIEGTLKNVLGSYGYSEIRLPIVEQTPLFKRAIGEVTDVVEKEMYTFEDRNGDSLTLRPEGTA  85
Tt  MTARAVRGTKDLFGKELRMHQRIVATARKVLEAAGALELVTPIFEETQVFEKGVGAATDIVRKEMFTFQDRGGRSLTLRPEGTA  84

                                        M2
Sa AVVRSYIEHKMQGNPNQPIKLYYNGPMFRYERKQKGRYRQFNQFGVEAIGAENPSVDAEVLAMVMHIYQSFGL.KHLKLVINSVG 167
Ec GCVRAGIEHGL..LYNQEQRLWYIGPMFRHERPQKGRYRQFHQLGCEVFGLQGPDIDAELIMLTARWWRALGISEHVTLELNSIG 168
Tt AMVRAYLEHGM.KVWPQPVRLWMAGPMFRAERPQKGRYRQFHQVNYEALGSENPILDAEAVVLLYECLKELGL.RRLKVKLSSVG 167

                                     I
Sa DMASRKEYNEALVKHFEPVIHEFCSDCQSRLHTNPMRILDCKVDRDKEAIKTAP..RITDFLNEESKAYYEQVKAYLDDLGIPYI 250
Ec SLEARANYRDALVAFLEQHKEKLDEDCKRRMYTNPLRVLDSKNPEVQALLNDAP..ALGDYLDEESREHFAGLCKLLESAGIAYT 251
Tt DPEDRARYNAYLREVLSPHREALSEDSKERLEENPMRILDSKSERDQALLKELGVRPMLDFLGEEARAHLKEVERHLERLSVPYE 252

          HisA              V          HisB
Sa  EDPNLVRGLDYYTHTAFELMMDNPNYDGAITTLCGGGRYNGLLELLDGPSETGIGFALSIERLLLALEE 319
Ec  VNQRLVRGLDYYNRTVFEWVTNS...LGSQGTVCAGGRYDGLVEQLGGRATPAVGFAMGLERLVLLVQA 317
Tt  LEPALVRGLDYYVRTAFEVHHEE...IGAQSALGGGGRYDGLSELLGGPRVPGVGFAFGVERVALALEA 318
```

FIGURE 4: Conformational differences in the active site. Both figures were generated by the same superposition mentioned in the legend of Figure 3. (A) Superposition of the HisA motif loops. The apo structure is blue and the HisRS−histidine complex yellow (bound histidine is orange), and hydrogen bonds are represented by dashed lines. (B) Structure of the active site. The apo structure is blue and the histidine complex yellow. Histidine, ATP, and Trp19 are modeled (all red) to orient discussions. The HisA motif, SI loop, motif 2 loop, loop of residues 273−280, Trp19, and the N-terminus are labeled as A, SI, M2, V, W, and N, respectively. (C) Structure-assisted sequence alignment of the three HisRS catalytic domains (*Sa*, *S. aureus*; *Ec*, *E. coli*; and *Tt*, *T. thermophilus)*. The various motifs and loops mentioned in the discussions are underlined. Red indicates residues that are identical in all three HisRS, while blue indicates residues that are identical between either *S. aureus* and *E. coli* or *S. aureus* and *T. thermophilus*.

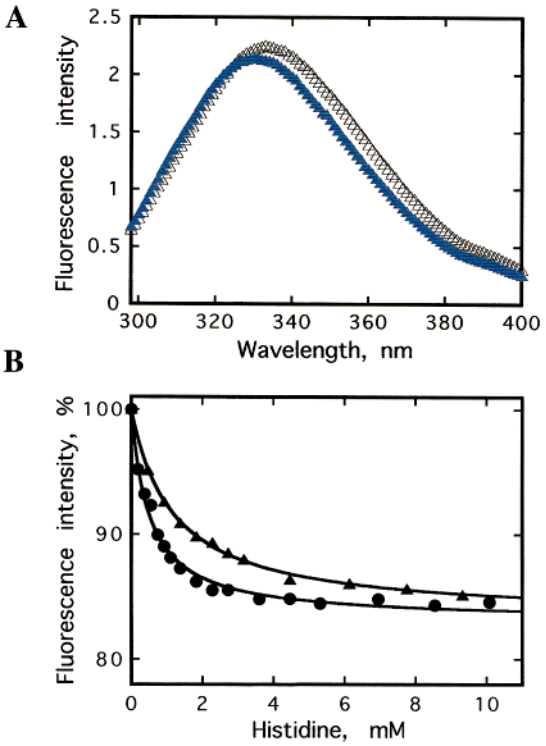

FIGURE 5: (A) Fluorescence spectra of HisRS. The line of black triangles was recorded with an excitation wavelength of 290 nm; the line of solid blue triangles represents the spectra of HRS following addition of 5 mM histidine. (B) Titration of HisRS with histidine. HisRS [50 μg/mL in 20 mM Tris (pH 8.0), 0.1 M NaCl, and 10 mM $MgCl_2$] was titrated with increasing amounts of histidine. Results are presented as fluorescence intensity at 350 nm with excitation at 290 nm. The symbols ▲ and ● represent data for histidine alone and histidine and AMP-PNP, respectively.

IIb synthetases (*12*−*14*). ATP-induced ordering of the motif 2 loop has also been reported in *T. thermophilus* HisRS (*7*), AspRS (*12*) and SerRS (*15*). We think ligand binding induces significant conformational changes for the HisA, SI, and motif 2 loops and the insertion domain, and our fluorescence data also support this view.

Cooperative Structural Dynamics. Our structural and fluorescence data suggest a significant ligand-induced conformational change of the HisA motif. It is interesting, however, that the only tryptophan of *S. aureus* HisRS, Trp19, is at least 16 Å away from the bound histidine (Figure 4B). Thus, analysis of the HisRS structures must reveal the relay mechanism by which histidine binding can transmit structural changes 16 Å away to Trp19. Looking from the left of Figure 4B, one can see that Trp19 is about 9 Å away from the closest ATP moiety. Although it is not impossible that Trp19 is affected by the ATP binding indirectly through residues situated between them, such a *tour-de-force* route seems unlikely for transmitting histidine-induced structural changes. On the other hand, when Figure 4B is viewed from its right, Trp19 can be easily correlated to the movement of the SI motif because it is very close to the N-terminal loop (Met1−Leu12). In fact, the helix where Trp19 resides shows enough differences between the apo and liganded structures (Figure 4B) that it may best explain our fluorescence data. Therefore, the drastic change in the HisA motif upon histidine binding can affect Trp19 through the cooperative movement of the SI motif. Since ATP or AMP-PNP appears to enhance the histidine binding affinity (K_d), it is reasonable to assume that the SI motif, situated between the histidine and ATP binding sites, is important in governing the communication between the two sites.

Figure 6 illustrates a plausible model for summarizing the above discussion. ATP-induced ordering of the motif loop is the only notable conformational change in all the reported HisRS structures (*5*−*7*), while histidine-induced changes are the main subject of this report. As histidine binds HisRS, there is a significant structural change in the HisA loop which forms a closed conformation of the binding pocket. By maintaining the numerous contacts, the insertion domain would also move with the HisA loop to be closer to the active site. Since the insertion domain is likely to interact with tRNA, the binding of histidine seems to set the stage for subsequent reactions. The incoming HisA motif loop could attract the SI loop and re-establish direct contacts between the two loops as seen in ligand-bound structures (*5*−*7*). The movement of the SI loop would affect the orientation of the entire SI motif, and hence the dimer interfaces as well. The change in the SI loop could also have direct functional implications, e.g., placing it in position to bind $tRNA^{His}$. Once the SI loop is in position, it may interact with the motif 2 loop, which will become ordered in the presence of the adenosine moiety to promote catalysis. In the absence of a HisRS−ATP complex structure, we postulate that the binding of ATP alone is sufficient to order the motif 2 and SI loops, but not sufficient to stabilize a preformed histidine-binding

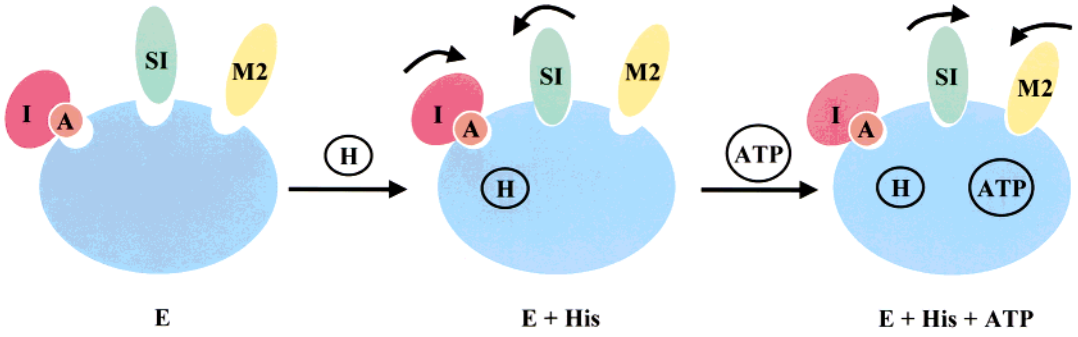

FIGURE 6: Ligand-induced structural changes in the HisRS active site. The insertion domain, HisA motif, small interface motif, and motif 2 loop are labeled as I, A, SI, and M2, respectively. The scene on the left shows the enzyme-only state (E) in an open conformation. The scene in the middle is with histidine bound, where the HisA motif, insertion domain (I), and SI motif move closer to the active site. The scene on the right is after the addition of ATP, where the motif 2 (M2) loop and SI motif are further stabilized.

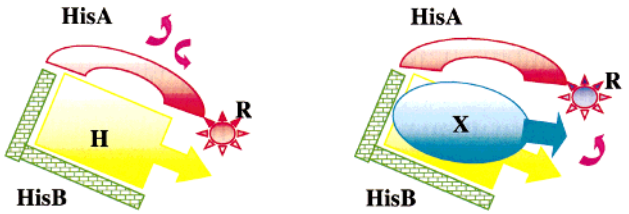

FIGURE 7: Proposed fidelity mechanism using cooperative dynamics. The HisB motif is shown as green blocks and is in a stable conformation. The yellow box with an arrow (H) represents the binding mode for the histidine ligand. The HisA motif is shown as a red arc and is highly dynamic. The star (R) represents Arg257. The scene on the left depicts the high-energy cost for stabilizing the histidine binding pocket. The scene on the right proposes that the catalytic Arg257 is misplaced (blue) when an incorrect ligand (X) is bound so that the catalysis of the wrong ligand is impaired.

pocket. It is unclear whether there is any functional role for the Asn273−Ile280 loop, but all the other changes in conformation seem to be highly correlated in our model. Therefore, we think that the structural dynamics in HisRS are not only considerable in magnitude but also highly cooperative in nature.

A Novel Fidelity Mechanism. There are two known mechanisms for improving charging fidelity (*1*). One of them uses a preformed and well-defined amino acid binding pocket. For example, TyrRS has a pocket that provides sufficient affinity differences to discriminate between tyrosine and the closely related phenylalanine (*1*); GlnRS uses additional elements from tRNA to establish the amino acid binding pocket (*16*). IleRS illustrates the other mechanism, in which the rigid amino acid binding site does not provide enough discrimination against valine. Therefore, a hydrolytic editing domain has evolved to correct these errors in IleRS (*1*). We think the dynamic HisA motif in HisRS offers a third novel fidelity mechanism.

Histidine is one of the most critical amino acids in proteins, found often as a catalytic residue (*17*) or a ligand for metals (*18*). A high degree of accuracy for charging $tRNA^{His}$ with the correct amino acid is thus very important. We have showed that HisRS recognizes the histidine ligand partly through a dynamic HisA motif. The HisA motif contains three important residues, Arg257, Tyr261, and Tyr262. The arginine, strategically positioned between the histidine and ATP, is essential for catalysis (*6*). The two tyrosines make hydrogen bonds to the histidine ligand (Figure 4A). The positioning of Arg257 is correlated to the two tyrosines because Arg257 is within the same HisA motif and makes a hydrogen bond to Tyr262 in all HisRS structures. This is interesting because it indicates that Arg257 is not in the proper position to undertake catalysis in the absence of a bound histidine ligand. Thus, for mischarging to occur, the incorrect amino acid might have to overcome two major obstacles. One is to afford sufficient binding energy to stabilize the dynamic HisA motif (left of Figure 7). This would reject many incorrect ligands considering a mere 1.2 mM K_d even for histidine at this highly optimized histidine binding pocket. The other requires the incorrect ligand to induce exactly the same conformation change for the proper positioning of Arg257 (right of Figure 7). Without this concerted structural change, the incorrect ligand will not be activated efficiently even with good binding affinity. This model is in agreement with known binding properties of various histidine analogues (*19*). We have not found any literature data to suggest whether HisRS is more or less discriminatory than aminoacyl-tRNA synthetases that use other fidelity mechanisms. Since the coupling of Arg257 and the mobile HisA motif is conserved and unique to HisRS, we believe it provides a likely mechanism for achieving sufficient fidelity in histidyl-tRNA synthetases.

Implications in Catalysis and Product Release. Some degree of cooperative dynamics is important in most enzymes (*19*), but a high energy cost is a consequence of having a highly flexible amino acid binding pocket. The fact that the pocket is rigid in most other synthetases indicates that the energy cost may be too high for many amino acids, especially the smaller ones. Histidine, on the other hand, can afford this cost because it can potentially interact with a protein in a number of different ways. For example, in ligand-bound HisRS structures, the histidine-binding pocket seems to be optimized to utilize the hydrogen bonding capabilities as well as the shape and electrostatic complementarity of histidine (*5*, *7*). Without the structural flexibility, one would have predicted a high binding affinity for histidine on the basis of this striking network of interactions. However, the observed K_d for histidine is only 1.2 mM in *S. aureus* HisRS, which suggests part of the binding energy has been used to order the mobile HisA loop. A much less exquisite histidine-binding pocket of the bacterial histidine-binding protein affords a K_d of 64 nM for histidine (*21*). When a 0.9 mM K_m for ATP is considered in *E. coli* HisRS (*6*), it is hard to believe that a more efficient enzyme could not have been designed. Although substrate binding and catalysis require some degree of cooperative dynamics in other synthetases (*12*−*15*), the large-scale cooperative dynamics proposed for HisRS must have evolved for other reasons.

As we discussed earlier, charging fidelity is probably one of the advantages offered by cooperative dynamics. Product release may be another. While the product of the amino acid

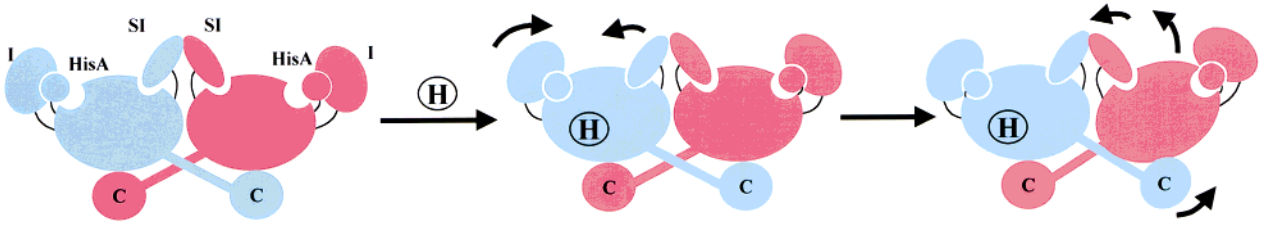

FIGURE 8: Model for domain communication in the HisRS dimer. Monomer 1 is blue and monomer 2 red. The left scene represents the ligand-free open conformation. The middle scene is when histidine (H) is bound to monomer 1, inducing movements in the HisA motif (HisA), the insertion domain (I), and the small interface motif (SI) of the monomer. The right scene is our proposed model, which indicates that the movements of the SI motifs could shift the core domain of monomer 2, and thus the C-terminal domain (C) of monomer 1.

activation step (i.e., histidyl-adenylate) need not be released, the final product (i.e., histidyl-$tRNA^{His}$) must be released from the enzyme and be escorted by elongation factors to the ribosome. Without significant active site dynamics, the product would have an affinity that was too high for it to be released from the deep and perfectly shaped histidine binding pocket. Using a low-affinity (i.e., imprecise) histidine binding pocket is not an option because there would not be enough specific interactions to ensure charging fidelity. Therefore, cooperative dynamics seem to be the best solution for HisRS catalysis since a perfect histidine pocket can be used to ensure fidelity and product release is no longer a problem. For example, once histidine is transferred onto tRNA from histidyl-adenylate, the byproduct AMP can be quickly released due to its low affinity and the intrinsically dynamic nature of the motif 2 loop. This may trigger the destabilization of the SI loop, HisA loop, and insertion domain, and allow the release of charged tRNA.

Interdomain Communication. All domains in HisRS are probably involved in tRNA binding. The catalytic domain has to bind the acceptor stem during the reaction. The insertion domain may be involved because of positional similarities between it and domains in other known class II synthetases. In our structure, a disordered loop (Asp207−Lys218) in the domain contains a conserved Lys209, which would be directly above the active site if the loop were to assume the same structure as in *T. thermophilus* HisRS (*7*), making it a likely candidate for interaction with tRNA. The SI motif may also be involved in tRNA binding using Lys62, while the C-terminal domain is in a reasonable position to bind the anticodon of tRNA. With all these domains to act upon a tRNA molecule, it is natural to expect some cooperativity in positioning these domains.

An interesting question is how the change in the N-terminal domain is transmitted into the C-terminal domain of the same monomer. A previous hypothesis is allosteric interactions by the relaxed loop that connects the two domains (*5*). By comparing the HisRS structures, we can suggest a more direct model for interdomain communication (Figure 8). We propose that all HisRS domains are designed to move swiftly in response to ligand binding. For example, monomer 1 will undergo a conformational change in its HisA motif upon histidine binding. This motion will pull its insertion domain near the active site. It will also move its SI motif closer to the active site through interactions with the SI loop (middle panel of Figure 8). As the SI motif of monomer 1 moves, so will the SI motif in monomer 2. Due to direct interactions between the SI motifs and catalytic cores, the core domain of monomer 2 could make a corresponding change (right panel of Figure 8). Because the C-terminal domain of monomer 1 directly contacts the core domain of monomer 2, its conformation could then change in concert with the initial ligand binding event in the monomer 1 catalytic core. It is known that mutations in the C-terminal domain at its interface with the core can compensate for unfavorable mutations in the tRNA discriminator base (*21*), which provides some support for our model. Further mutagenesis and biochemical experiments should and could be devised to confirm this model.

ACKNOWLEDGMENT

We thank Dr. Richard Jarvest for his continuous support and valuable suggestions for this work and Dr. Ward Smith for useful discussions. We thank Sally Gout, Jo Jones, and Dr. E. Imogen Wilding for expression and fermentation support. We also thank the IMCA-CAT (Industrial Macromolecular Crystallographic Association Collaborative Access Team) staff for assistance in data collection at the Advanced Photon Source.

REFERENCES

1. Fersht, A. (1985) *Enzyme Structure and Function*, Freeman & Co., New York.
2. Jakubowski, H., and Goldman, E. (1992) *Microbiol. Rev. 56*, 412−429.
3. Eriani, G., Delarue, M., Poch, O., Gongloff, J., and Moras, D. (1990) *Nature 347*, 203−206.
4. Cusack, S. (1995) *Nat. Struct. Biol. 2*, 824−831.
5. Arnez, J. G., Harris, D. C., Mitschler, A., Rees, B., Francklyn, C. S., and Moras, D. (1995) *EMBO J. 14*, 4143−4155.
6. Arnez, J. G., Augustine, J. G., Moras, D., and Francklyn, C. S. (1997) *Proc. Natl. Acad. Sci. U.S.A. 94*, 7144−7149.
7. Aberg, A., Yaremchuk, A., Tukalo, M., Rasmussen, B., and Cusack, S. (1997) *Biochemistry 36*, 3084−3094.
8. Collaborative Computational Project, No. 4 (1994) *Acta Crystallogr. A42*, 140−149.
9. Brunger, A. T. (1987) *X-PLOR Version 3.1, A system for X-ray crystallography and NMR*, Yale University Press, New Haven, CT.
10. McRee, D. E. (1993) *Practical Protein Crystallography*, Academic Press, San Diego, CA.
11. Kraulis, P. (1991) *J. Appl. Crystallogr. 24*, 946−950.
12. Poterszman, A., Delarue, M., Thierry, J. C., and Moras, D. (1994) *J. Mol. Biol. 244*, 158−167.
13. Cusack, S., Yaremchuk, A., and Tukalo, M. (1996) *EMBO J. 15*, 2834−2842.
14. Schmitt, E., Moulinier, L., Fujiwara, S., Imanaka, T., Thierry, J. C., and Moras, D. (1998) *EMBO J. 17*, 5227−5237.
15. Belrhali, H., Yaremchuk, A., Tukalo, M., Larsen, K., Berthet-Colominas, C., Leberman, R., Beijer, B., Sproat, B., Als-Nielsen, J., Grubel, G., Legrand, J. F., Lehmann, M., and Cusack, S. (1994) *Science 263*, 1432−1436.
16. Rath, V. L., Silvian, L. F., Beijer, B., Sproat, B. S., and Steitz, T. A. (1998) *Structure 6*, 439−449.
17. Qiu, X., Culp, J. S., DiLella, A. G., Hellmig, B., Hoog, S. S., Janson, C. A., Smith, W. W., and Abdel-Meguid, S. S. (1996) *Nature 383*, 275−279.
18. Karlin, S., Zhu, Z. Y., and Karlin, K. D. (1997) *Proc. Natl. Acad. Sci. U.S.A. 94*, 14225−14230.
19. Lepore, G. C., Di Natale, P., Guarini, L., and De Lorenzo, F. (1975) *Eur. J. Biochem. 56*, 369−374.
20. Carter, C. W., Jr. (1993) *Annu. Rev. Biochem. 62*, 715−748.
21. Yao, N., Trakhanov, S., and Quiocho, F. A. (1994) *Biochemistry 33*, 4769−4779.
22. Yan, W., Augustine, J., and Francklyn, C. (1996) *Biochemistry 35*, 6559−6585.

BI990482V